International Journal of Geo-Information

MDPI

Article

Comparing Characteristics of the Urban Thermal Environment Based on the Local Climate Zone in Three Chinese Metropolises

Riguga Su [1,2], Chaobin Yang [1,3,4,5,*], Zhibo Xu [1], Tingwen Luo [1], Lilong Yang [3], Lifeng Liu [3] and Chao Wang [3]

1 Key Laboratory of Urban Land Resources Monitoring and Simulation, Ministry of Natural Resources, Shenzhen 518040, China
2 College of Agricultural Engineering and Food Science, Shandong University of Technology, Zibo 255000, China
3 School of Civil Engineering and Geomatics, Shandong University of Technology, Zibo 255000, China
4 State Key Laboratory of Urban and Regional Ecology, Research Center for Eco-Environmental Sciences, Chinese Academy of Sciences, Beijing 100085, China
5 State Key Laboratory of Green Building in Western China, Xi'an University of Architecture & Technology, Xi'an 710055, China
* Correspondence: yangchaobin@sdut.edu.cn; Tel.: +86-156-6643-1881

Abstract: Urban landscape has important effects on urban climate, and the local climate zone (LCZ) framework has been widely applied in related studies. However, few studies have compared the relative contributions of LCZ on the urban thermal environment across different cities. Therefore, Beijing, Shanghai, and Shenzhen in China were selected to conduct a comparative study to explore the relationship between LCZ and land surface temperature (LST). The results showed that (1) both the composition and spatial configuration of LCZ had obvious differences among the three cities. Beijing had a higher area proportion of compact mid-rise and low-rise LCZ types. The spatial pattern of LCZ in Shenzhen was especially quite different from those of Beijing and Shanghai. (2) Shenzhen had the strongest summer surface urban heat island (UHI) intensity and the largest UHI region area. However, the proportion of urban cooling island areas was still the highest in Shenzhen. (3) Different LCZs showed significant LST differences. The largest LST difference between the LCZs reached 5.57 °C, 4.50 °C, and 12.08 °C in Beijing, Shanghai, and Shenzhen, respectively. Built-up LCZs had higher LSTs than other LCZ types. (4) The dominant driving LCZs on LST were different among these cities. The LST in Beijing was easily influenced by built-up LCZ types, while the cooling effects generated by LCZ G(water) were much stronger than built-up LCZs' warming effects in Shanghai. These results indicated that the effect of the LCZ on LST had significant differences among LCZ types and across cities, and the dominant LCZs should be given more priority in future urban planning.

Keywords: local climate zone; urban heat island; land surface temperature; urban climate; comparative analysis

check for updates

Citation: Su, R.; Yang, C.; Xu, Z.; Luo, T.; Yang, L.; Liu, L.; Wang, C. Comparing Characteristics of the Urban Thermal Environment Based on the Local Climate Zone in Three Chinese Metropolises. *ISPRS Int. J. Geo-Inf.* **2024**, *13*, 61. https://doi.org/10.3390/ijgi13020061

Academic Editors: Wolfgang Kainz and Godwin Yeboah

Received: 7 January 2024
Revised: 5 February 2024
Accepted: 15 February 2024
Published: 19 February 2024

Copyright: © 2024 by the authors. Licensee MDPI, Basel, Switzerland. This article is an open access article distributed under the terms and conditions of the Creative Commons Attribution (CC BY) license (https://creativecommons.org/licenses/by/4.0/).

1. Introduction

As the main habitat of human beings, cities are susceptible to more heat risks under the combined influence of rapid world urbanization and global climate changes [1–3]. Among these negative impacts caused by land cover and land use changes, the urban heat island (UHI) phenomenon, suggesting that urban areas have higher temperatures than the rural areas, has proven to produce a wide range of impacts on social–ecological issues, such as threatening public health, resulting in more energy costs from air conditioners, and causing severe urban air pollution [4–7]. It is projected that over two-thirds of the world's population will soon live in urban areas, indicating more people will be influenced by climate-related risks [8]. Therefore, to deal with these urban climate risks, there is a pressing need to deepen our knowledge about the spatial features of urban thermal environments and their potential driving factors.

UHI has been monitored and studied by three main methods: air temperature, land surface temperature (LST), and modeling simulation, where each approach has its own advantages and shortcomings [9,10]. Due to the complex spatial variability of urban landscapes and social–cultural differences, the urban thermal environment could vary significantly in a very short distance inside a city [11,12]. As a result, the data or method employed to measure urban climate should provide explicit spatial information on the thermal conditions. Consequently, surface UHI (SUHI) characterized by LST has been widely used by urban climate researchers [13–15]. Compared to traditional air temperature, the LST retrieved from thermal infrared remote sensing images can provide the temperature of each pixel across the whole study area [16]. Landsat images with higher spatial resolutions compared to MODIS were preferred in previous urban climate studies [17,18].

Many urban classification schemes have been proposed as analysis units to explore the urban climate [4,19–21]. However, these classification methods have not yet provided a uniform standard and simply rely on the traditional so-called urban and rural qualifiers. Fortunately, Stewart and Oke proposed a new "local climate zone" (LCZ) classification system as the urban research framework for urban climate studies [22]. The urban area was divided into ten built and seven land cover LCZ types, and each type had a range of certain geometric and surface cover property values [22]. Accordingly, the UHI studies could be calculated, compared, and explored scientifically across different cities. The fundamental basis of applying the LCZ framework was to generate high-quality LCZ maps. Typically, three main methods were used for LCZ mapping, including in situ measurement, GIS, and remote-sensing-image-based approaches [23–26]. Regarding the satellite-image-based method, the World Urban Databases and Access Portal Tools (WUDAPT) was a popular project to create consistent LCZ maps of global cities [27]. In particular, an LCZ generator web application was proposed to map cities into LCZs with the advantages of simple inputs, automated accuracy assessment, and identification of suspicious training areas [28]. In addition, the improvement will help urban climate scientists to ease the accessibility of high-quality LCZ maps.

Applications of the LCZ framework in UHI-related studies have become popular in recent research [29–31]. Numerous studies have examined the spatial–temporal features and impact factors of the thermal environment differences among different LCZ types [32–34]. The spatial patterns of nocturnal UHI were explored based on the LCZ framework in Hong Kong, and the results showed that in certain LCZs, high mean sky view factors and previous surface fractions were the most explanatory variables of local UHI [35]. The relationships between distributions of LCZs and surface temperatures were analyzed in cities in the Yangtze River Delta, and the results showed that low-rise buildings were mostly aggregated and obvious differences were observed between the LST and various LCZs [36]. Furthermore, diurnal dynamics of heat exposure characterized by the LST in Xi'an, China was discussed from the perspective of the LCZ, and the results indicated that compact built-up LCZs had much higher LSTs over the day [37]. A case study in Tehran, Iran explored the correlations between LST and space syntax using the LCZ, where the results showed that bare soil and water had the lowest and highest LSTs, respectively [38]. It cannot be denied that previous studies have advanced the development and applications of LCZs in urban climate research. However, there still exist several deficiencies in the exploration of relationships between LCZ and LST. First, most of these studies focused on a single city, while the characteristics of a LCZ might have variations among cities, and thus produced different influences on LST. Therefore, it is essential to conduct a comparative study to obtain a comprehensive understanding of the relationships between LCZ and LST. Second, when exploring the effect of LCZ on the urban thermal environment, few studies have considered the potential influence of different compositions of LCZs on LST. Most of the current studies just compared the LST differences among LCZ types. Third, among 17 LCZs, what are the potential dominant driving factors on the variations of LST? Are the dominant factors the same or different across cities? Few studies have answered these questions.

Therefore, given the mentioned gaps in the current literature, three metropolises including Beijing, Shanghai, and Shenzhen in China were selected as study areas. The primary goals of this study are to (1) explore the composition differences and spatial patterns of LCZs in the three cities; (2) assess the relationships between LCZ and LST and examine the potential variations of these relationships among cities; and (3) compare the relative contributions of different LCZs on the urban thermal environment and thus determine the dominant LCZ types affecting LST. It is hoped that our results will add new knowledge pertaining to the effects of LCZ on urban climate and provide a scientific basis for future urban planning and better climate adaptation strategies.

2. Materials and Methods

2.1. Study Area

China has experienced irreversible urbanization and industrialization since the beginning of the 21st century, with the urban population increasing from 36.22% in 2000 to 65.22% in 2022 (https://www.stats.gov.cn/sj/ndsj/2023/indexch.htm) (accessed on 4 February 2024); consequently, several megacities have emerged all over the country. Aiming at contrasting urban landscapes and their potential different effects on the urban thermal environment, this study selected three megacities in China: Beijing, Shanghai, and Shenzhen (Figure 1). These three cities are characterized by varied urban morphology, different climate features, and diverse cultures, making them ideal study areas for comparative research.

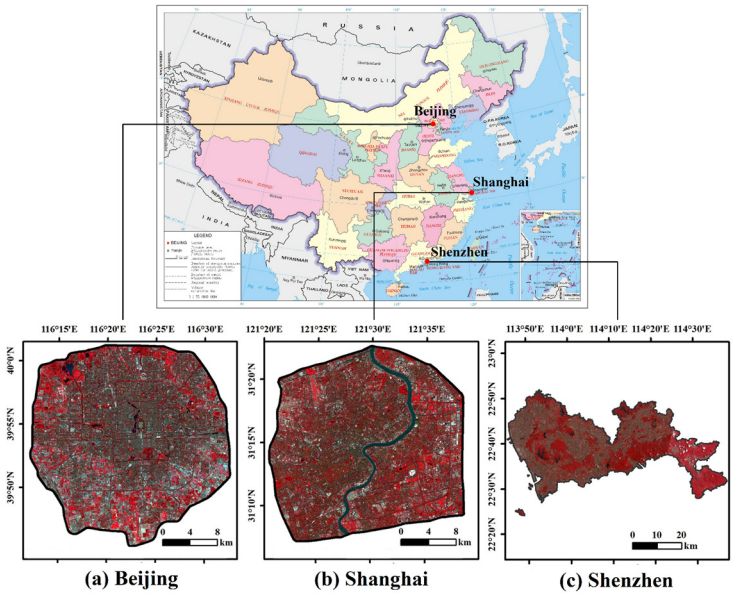


Figure 1. The locations of (**a**) Beijing, (**b**) Shanghai, and (**c**) Shenzhen in China.

Beijing, the capital of China, located in the North China Plain, is the political and cultural center of the country and a famous modern international city with a long history. It has a warm, temperate climate with a hot rainy summer and a cold, dry winter [39]. Compared to the other two cities, Beijing has a historical city center and many ancient buildings and is easily influenced by top–down central government policies, which might produce unique impacts on LST. Shanghai, a coastal city, is the economic and financial center of China. It is characterized by a northern subtropical monsoon climate with an average annual temperature of 17.2 °C. There are numerous small rivers and ditches inside Shanghai city, which makes it unique for urban thermal environment studies [40]. Shenzhen is a newer, built-up modern international metropolis, and signaled the beginning of the reform and opening up of China. Adjacent to Hong Kong, Shenzhen is a coastal city on the east bank of the Pearl River Estuary and characterized by a subtropical monsoon climate with an annual average temperature of 23.0 °C.

2.2. Data Sources

The World Urban Database and Access Portal Tools (WUDART) project is a community-based project to facilitate urban-focused climate, weather, and energy-use modeling application studies around the world (https://www.wudapt.org) (accessed on 12 December 2023). As a part of WUDART, a protocol was developed to ease the workflow of researchers in mapping a city of interest into LCZs [28]. Therefore, three filtered LCZ maps for Beijing, Shanghai, and Shenzhen were downloaded from the following official website (https://www.wudapt.org/lcz-maps/) (accessed on 8 November 2023) where they were created by a LCZ generator [28]. All the employed LCZ datasets in our study are distributed under the CC BY-NC-SA 4.0 license, which guarantees the consistency and comparability of the LCZ maps. The detailed information of the LCZ maps can be found in Table 1.

Table 1. Data used in this study.

	LCZ Maps			Landsat 8 OLI/TIRS	
	ID	**OA**	**SR**	**ID**	**SR**
Beijing	f176fa1d6a5d1bf4a4fbf87f586f041f53afbb62	0.81	100 m	LC81180382019242LGN03	30 m
Shanghai	4d75af7c4517d21b8d6c9fbdb847e890948968b6	0.82	100 m	LC81180382020229LGN00	30 m
Shenzhen	9947aa626033e2a56a662c1477adfd32421c5317	0.62	100 m	LC08_L2SP_121044_20210723_20210729_02_T1 LC08_L2SP_122044_20230602_20230607_02_T1	30 m

OA: overall accuracy. SR is short for spatial resolution.

Landsat 8 images were selected in our study to generate summer LST maps for spatial analysis of urban thermal environment due to their high quality and wide applications in previous and current urban heat islands studies [18,41]. Three cloud-free Landsat 8 images were obtained from USGS and preprocessed by radiometric correction and co-registration in the ENVI 5.5 before LST retrievals. In addition, Google Earth images, local weather station records, and Baidu Street View Map were used as supplementary data for LCZ recognition and the validation of LST.

2.3. Methods

2.3.1. LCZ Classification

The most popular LCZ framework was proposed in 2012 by Stewart and Oke, where LCZ were defined as regions of uniform surface urban landscapes and human activity that range from several hectares to square kilometers [22]. The urban area is divided into 17 LCZ types, in which LCZs 1–10 are built types and LCZs A–G are land cover types (Table 2) [22]. Although the LCZ system provides a new generic research framework, it cannot depict the characteristics of every urban site due to the diversity of cities [26]. Therefore, not all the 17 LCZ types were included in our study area, as Beijing did not have LCZ 10 and Shanghai had no LCZ 7, while Shenzhen had no LCZ 7, 9, or C, based on their local current situations.

2.3.2. LST Retrieval

The LST is usually retrieved from Landsat 8 TIRS bands by applying a single-window algorithm or the radiation correction equation [14]. Based on previous studies, the LST can be obtained based on the following formula:

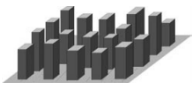
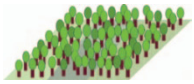
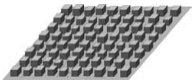
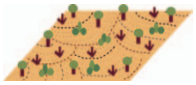
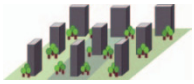
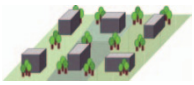
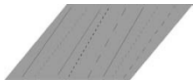
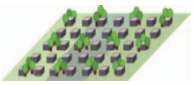
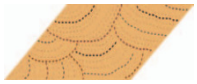
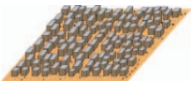
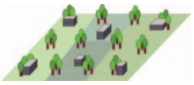
$$\mathrm{LST} = \frac{\mathrm{Tb}}{1 + (\lambda \mathrm{Tb}/\rho)\ln \varepsilon}$$

where λ is the wavelength of band 10 (=10.9 μm) for Landsat 8, $\rho = 1.43 \times 10^{-2}$ mK. ε is the land surface emissivity (LSE), a very important parameter that determines the accuracy of retrieved LST [42]. Typically, the LSE is estimated by the NDVI threshold method. Tb is the bright temperature (BT), an effective temperature under the assumption that the whole earth is a emissivity unity, and can be calculated as follows:

$$T_b = K_2/\ln(K_1/\mathrm{Radiance} + 1)$$

where the values of K_2 and K_1 can be found in the metadata of Landsat images and the radiance can be converted from the original digital number (DN) according to the Landsat 8 Data USERS HANDBOOK [43].

Table 2. Description of the 17 LCZ types.

Built-Up LCZ		Land Cover LCZ	
LCZ 1: Compact high-rise		LCZ A: Dense trees	
LCZ 2: Compact midrise		LCZ B: Scattered trees	
LCZ 3: Compact low-rise		LCZ C: Bush, scrub	
LCZ 4: Open high-rise		LCZ D: Low plants	
LCZ 5: Open mid-rise		LCZ E: Bare rock or paved	
LCZ 6: Open low-rise		LCZ F: Bare soil or sand	
LCZ 7: Lightweight low-rise		LCZ G: Water	
LCZ 8: Large low-rise			
LCZ 9: Sparsely built			
LCZ 10: Heavy industry			

Detailed information can be found in the original literature [22].

2.3.3. Indicators for SUHI Intensity

SUHI intensity is defined as the LST difference between urban and rural areas [44]. However, few studies have estimated the SUHI intensity from the perspective of the LCZ framework. Therefore, three new SUHI intensity indicators including Mean_SUHI (MSUHI), Strongest_SUHI (SSUHI), and Representive_SUHI (RSUHI) are proposed in our study based on previous studies and the following principles: (1) they are easily understood and estimated; and (2) they hold scientific and practical importance [44,45]. Table 3 shows the detailed information of the three SUHI intensities. The LSTs for different LCZ types was calculated via using the "Zonal" Spatial Analysis Tool in ArcGIS 10.8.

Table 3. The three SUHI intensity indicators which are proposed in this study.

Indicator (Abbreviation)	Calculation	Description
Mean_SUHI (MSUHI)	Mean LST (built LCZ types) − Mean LST (landcover LCZ types)	reflect the average SUHI intensity for the whole study area
Strongest_SUHI (SSUHI)	Max LST (built LCZ type) − Min LST (landcover LCZ type)	reflect the largest LST difference among different LCZ types
Representive_SUHI (RSUHI)	LST (max size built LCZ type) − LST (max size landcover LCZ type)	reflect the reprehensive LST difference among LCZ types based on their corresponding largest area

2.3.4. Statistical and Spatial Analysis

To explore the effect of LCZ on the urban thermal environment, 1 km × 1 km grids were created for the three studied cities by applying the ArcGIS fishnet tool. Considering the 100 m resolution of LCZ maps and resembled 30 m Landsat TIRS images, each 1 km × 1 km grid could cover 100 LCZ pixels and over 1000 LST pixels, which could be taken as a small "landscape". There are 717, 715, and 2184 grids in total for Beijing, Shanghai, and Shenzhen, respectively. First, Spearman's rho correlation analysis was used to explore the relationship between the area of LCZ and LST due to their abnormal distributions. Second, linear regression models were constructed to examine the relative contributions of different LCZ types to the variations of LST. The area of different LCZ was considered as an independent variable, while the average LST of each analysis unit grid was set as a dependent variable. The β in these models was used to compare the relative contributions of each variable for each city, while the adjusted R^2 was applied to compare the performance of these models. All the statistical analyses were conducted with the help of SPSS 22.0.

3. Results

3.1. Spatial Pattern of LCZ

The spatial distributions of different LCZs for Beijing, Shanghai, and Shenzhen are shown in Figure 2. The areas of Beijing and Shanghai in this study were similar in size, while their spatial patterns of LCZ had obvious differences. By comparing Figure 2a,b, it can be seen that the LCZs 1–3 (compact built types), characterized by a red color, cover much more area in Beijing (46.06%) than that in Shanghai (19.03%), which is also shown in Figure 3. LCZ4 (19.91%) and LCZ5 (20.73%) are the dominant LCZ types in Shanghai. Figure 3 also shows that Shanghai (89.28%) has the largest area of built LCZs compared with Beijing (82.79%) and Shenzhen (54.70%). In addition, as a coastal city, the area of LCZ G in Shanghai (3.76%) was 2.5 times larger than that in Beijing (1.50%). Most of the land cover LCZ types were located in the periphery of the city, which was consistent in both Beijing and Shanghai.

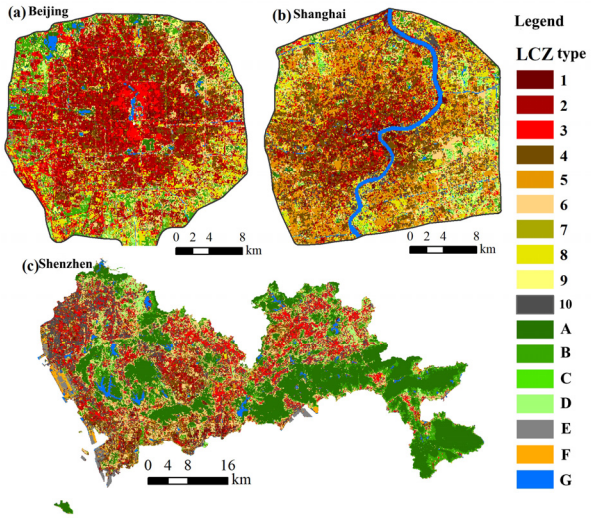


Figure 2. Spatial patterns of LCZs in (**a**) Beijing, (**b**) Shanghai, and (**c**) Shenzhen.

Different from Beijing and Shanghai, where the city core was taken as the study area, the administrative scope of Shenzhen was considered in our study because it was difficult to find a freeway covering the downtown. Therefore, the spatial pattern of LCZ in Shenzhen was quite different from the other two cities. Typically, most of the built-type LCZs were located in the west and central part of Shenzhen, and there still simultaneously existed large land cover LCZ types in these regions. For built LCZ types, LCZ 6, LCZ 4, and LCZ 3 were the three largest types. LCZA was the largest LCZ type in Shenzhen, and the land cover LCZ types cover almost half of the study area, indicating it is a city with very high

vegetation coverage. As a result, by comparing Figures 2 and 3, it was clear that both the component composition and spatial configuration of LCZ exhibited obvious differences that might be due to the variations in history, culture, climate, and policies.

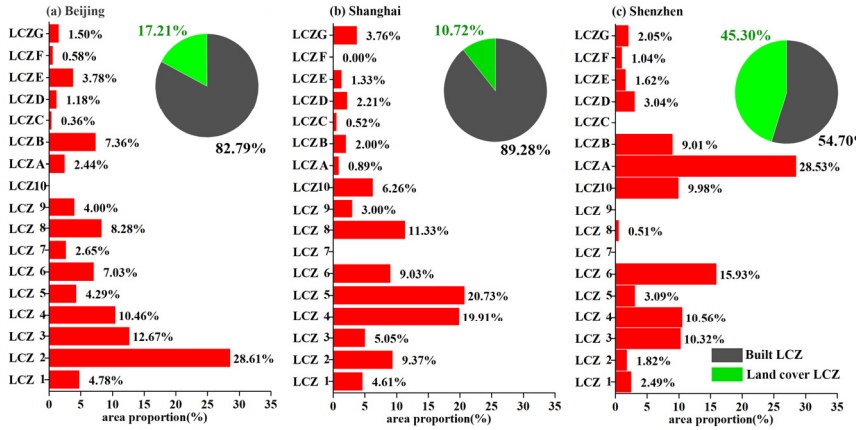


Figure 3. Statistical information of LCZs in (**a**) Beijing, (**b**) Shanghai, and (**c**) Shenzhen.

3.2. Spatial Patterns of LST

Overall, the spatial distributions of summer LST for Beijing, Shanghai, and Shenzhen were consistent with patterns of LCZs, as can be seen by comparing Figures 2 and 4, where built-up LCZs are shown to have had higher temperatures than land cover LCZs. The red color represents high LSTs in Figure 4, and the results indicated that there were obvious UHI pheromones in these three cities where low temperatures were usually found in the surrounding area of the city core. For Beijing, the highest LSTs were located in the downtown Tian An Men Square and the southwest part due to the large area of artificial impervious surfaces. For Shanghai, clustered quays along the Yangtze River in the northeast part were the hottest areas, while Shenzhen Baoan International Airport and bare sand or the sites under construction in the west coastline had the highest LST. The low-temperature area was associated with water bodies and vegetation due to their cooling effect. For the statistical characteristics, the average LSTs for Beijing, Shanghai. and Shenzhen were 32.10 °C, 33.38 °C, and 36.16 °C, respectively. Shanghai had the lowest temperature difference due to its higher minimum LST than Beijing and Shenzhen, which had the largest LST range (53.47 °C).

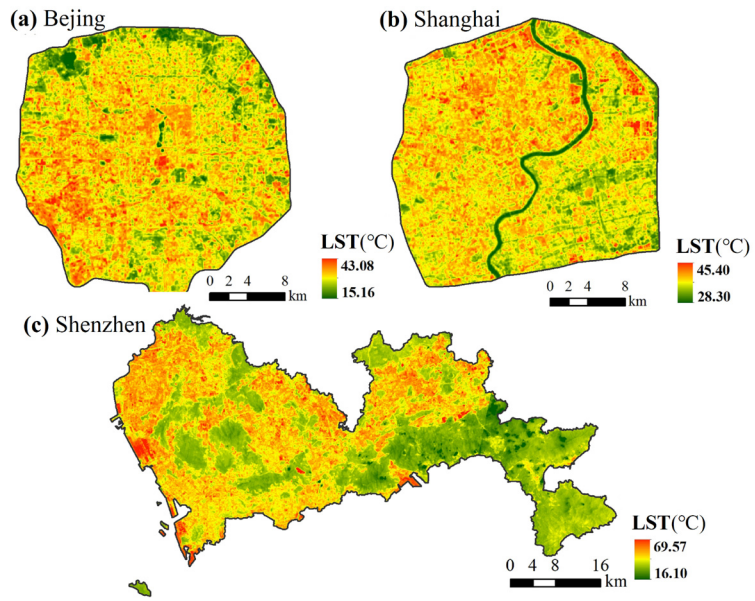


Figure 4. Spatial distributions of LST in (**a**) Beijing, (**b**) Shanghai, and (**c**) Shenzhen.

3.3. LST Differences among LCZs and SUHI Intensity

The average, highest, and lowest LST for each LCZ type in Beijing (gray), Shanghai (red), and Shenzhen (blue) are shown in Figure 5 by using the Zonal tools in ArcGIS 10.8. For the LST differences among cities, the average LST for all LCZ types in Shenzhen was the highest, followed by Shanghai and Beijing. An interesting phenomenon was that the minimum LST for each LCZ in Shanghai had the largest values, while Shenzhen had the lowest minimum LST (Figure 5b). Shenzhen had the largest maximum LST that was much higher than Beijing and Shanghai, where the maximum LST differences in the two cities were not that significant. However, it should also be noted that the maximum and minimum LST for LCZ might have some uncertainties. Therefore, the average LST was used to compare the temperature difference among LCZ types.

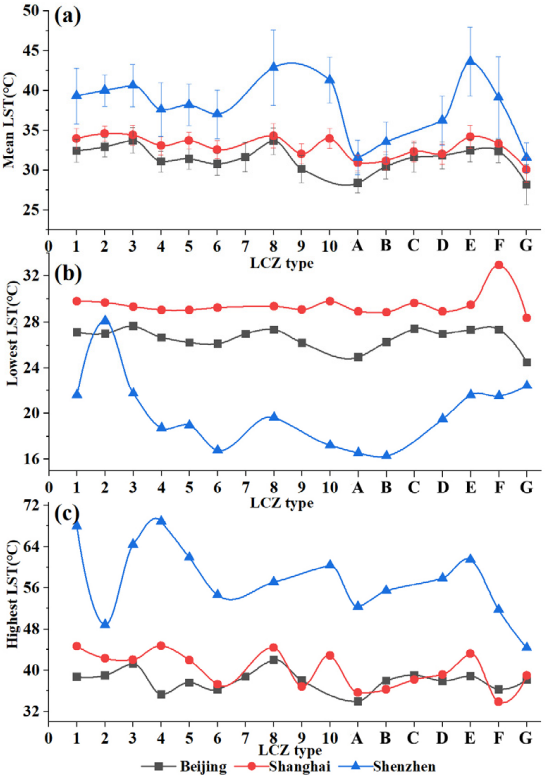


Figure 5. The (**a**) mean, (**b**) lowest, and (**c**) highest LSTs among LCZs in three cities.

There existed huge average LST variations across different LCZ types, as shown in Figure 5a. Typically, built-up LCZs had much higher LSTs than land cover LCZs, except for LCZ E, which consisted of bare rock or an artificial impervious surface. LCZs 2, 3, and 8 were the three hottest LCZ types in Beijing and Shanghai, while LCZs E (43.67 °C), 8 (42.88 °C), and 10 (41.30 °C) had the highest LSTs in Shenzhen. Furthermore, Figure 5b,c also indicate that the variations of LST among LCZs had similar characteristics in both values and changing trends for Beijing and Shanghai, which was different from that in Shenzhen. LCZ A and LCZ G were the coldest LCZ types in all three cities. For LCZs 1–3, Figure 5a showed that LCZ 3 had the highest LST, indicating that building height tended to have a negative effect on the LST when they had similar compact building densities. However, this was not applied to LCZs 4–6, where the building surface fraction in these LCZs was between 20 and 40%. In this case, LCZ 5 was the hottest, and LCZ 6 with low-rise buildings had the lowest LST. Therefore, it could be inferred that the relationship between buildings and LSTs is complicated. A consequent and very interesting question emerged: which impact factor has a larger influence on LST, building density or building height?

The results of three different indicators for SUHI intensity in Beijing, Shanghai, and Shenzhen are shown in Figure 6. SUHI intensity can help quantitatively characterize the

severity of the urban thermal environment. MSUHI was an indicator to examine the mean LST difference between built and land cover LCZs in this study, and Figure 6 shows that Shenzhen had the largest MSUHI intensity (6.12 °C), which was much stronger than Beijing (1.83 °C) and Shanghai (2.26 °C). SSUHI represents the largest LST difference among LCZs, and Shenzhen still had the largest SSUHI, which was followed by Beijing and Shanghai. When it comes to RSUHI, Beijing had the smallest value.

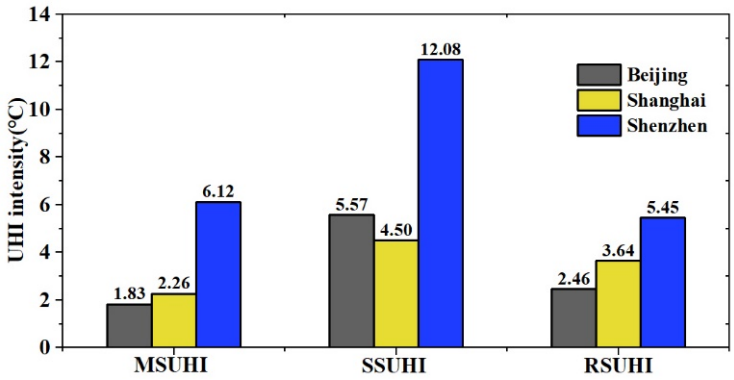


Figure 6. Three different SUHI indicators of the studied cities.

3.4. Relationships between LCZ and LST

As mentioned in Section 2, the 1 km × 1 km grid in our study was taken as the basic statistical analysis unit. Due to the definition stating that LCZs are regions of uniform urban landscape, the LCZ was considered as a whole impact factor without conducting an exploration of its inner components. In other words, the LCZ was the fundamental composition element for each grid.

Based on this consideration, the results of the Spearman's rho between LCZ and LST for the three cities are shown in Table 4. Most of the built LCZs have positive relationships with LST, except for LCZ 6 and LCZ 9, and land cover LCZ had negative correlations with LST excluding LCZ E and LCZ G. Although LCZ 6 is a built-up LCZ, it had negative relationships with LST in Beijing and Shanghai. The possible reason was that these LCZs had few low-rise buildings and relatively high coverages of vegetation. When comparing the intensity of relationships between LST and built-up LCZs, it was found that there existed obvious differences among these three cities. For Beijing, LCZ 2 and LCZ 3 had the strongest correlations with LST, while the corresponding LCZ types were LCZ 2 and LCZ 1 in Shanghai. For Shenzhen, LCZ 10 and LCZ 3 had the strongest warming effect. Overall, the relationships between LCZ and LST were much stronger in Shenzhen than in Beijing and Shanghai. For the correlation between land cover LCZs and LST, LCZs A, B, and G showed strong negative effects on LST in these three cities. Therefore, it could be inferred that the relationships between LST and land cover LCZs did not have significant differences in the three cities as their inter compositions had few differences. However, the relationships between LST and built LCZs were more complicated due to the variations in interior structures.

Table 4. The correlation coefficients between LCZ and LST for Beijing, Shanghai, and Shenzhen.

	LCZ 1	LCZ 2	LCZ 3	LCZ 4	LCZ 5	LCZ 6	LCZ 7	LCZ 8	LCZ 9	LCZ 10
Beijing	0.201 **	0.517 **	0.474 **	0.081 *	00.213	−0.457 **	−0.045	0.319 **	−0.45 **	--
Shanghai	0.349 **	0.571 **	0.153 **	0.058	0.217 **	−0.467 **	--	0.102 **	−0.372 **	0.091 *
Shenzhen	0.564 **	0.494 **	0.746 **	0.471 **	0.507 **	0.348 **	--	0.325 **	--	0.762 **
	LCZ A	**LCZ B**	**LCZ C**	**LCZ D**	**LCZ E**	**LCZ F**	**LCZ G**			
Beijing	−0.548 **	−0.373 **	−0.056	−0.042	0.002	0.052	−0.400 **			
Shanghai	−0.227 **	−0.423 **	−0.102 **	−0.328 **	0.112 **	0.031	−0.308 **			
Shenzhen	−0.786 **	−0.406 **	--	0.09 **	0.373 **	0.101 **	−0.187 **			

** $p < 0.01$ (two-tailed). * $p < 0.05$ (two-tailed).

The multilinear regression results of LCZs and LST for the three studied cities are shown in Table 5 where beta represented the relative contributions to the variations of LST. The red and blue colors indicate positive and negative values, respectively. There were obvious differences in the number and types of LCZs that entered the regression models. For Beijing, LCZs 2, 3, and 8 had the largest contributions to the high LSTs, while LCZs G, 9, and A had significant cooling effects. Twelve of the seventeen LCZ variables entered Shanghai's regression model, and the cooling effect generated by LCZ G was much stronger than other land cover LCZs, such as LCZ A and LCZ B. However, the contribution of built LCZs to warming LST, such as LCZ 2 and LCZ 3, was much smaller compared to the negative contributions generated by land cover LCZ types. LCZ A had the largest negative contributions to LST in Shenzhen, and LCZs 10, E, and 3 had relatively high positive effects on LST. Although Shenzhen has many more analysis grids than Beijing and Shanghai, its adjusted R^2 (0.803) was similar to Beijing (0.804), which was higher than Shanghai (0.710). Based on these results, we found that the dominant impact factors (or LCZ types) on LST at the grid spatial scale were different in these three cities.

Table 5. Regression results of LCZ and LST.

	Beijing		Shanghai		Shenzhen	
	β	Sig.	β	Sig.	β	Sig.
LCZ 1						
LCZ 2	0.470	0.00	0.190	0	0.063	0.00
LCZ 3	0.388	0.00	0.055	0.010	0.177	0.00
LCZ 4			−0.252	0.00		
LCZ 5					0.040	0.001
LCZ 6			−0.332	0.00		
LCZ 7						
LCZ 8	0.349	0.00	0.125	0.00	0.053	0.00
LCZ 9	−0.143	0.00	−0.195	0.00		
LCZ 10					0.189	0.00
LCZ A	−0.186	0.00	−0.121	0.00	−0.519	0.00
LCZ B			−0.184	0.00	−0.176	0.00
LCZ C			−0.100	0.00		
LCZ D	0.082	0.00	−0.126	0.00	−0.028	0.007
LCZ E	0.128	0.00	0.068	0.002	0.181	
LCZ F					0.025	0.014
LCZ G	−0.175	0.00	−0.544	0.00	−0.148	
Constant	30.240		34.010		36.925	
R^2	0.805		0.715		0.804	
Adjusted R^2	0.802		0.710		0.803	

The color in the table indicates the value of β, where the color scales of red and blue represent high positive and negative values, respectively.

4. Discussion

4.1. Differences in the Spatial Patterns of LCZs

The access to accurate LCZ maps for the studied area was the basis for conducting the following exploration of their spatial patterns and effects on the urban thermal environment [26]. In this study, three LCZ maps produced by the LCZ Generator for Beijing, Shanghai, and Shenzhen were obtained as the main data sources. Despite these maps being downloaded from an open-source website, they had good consistency in the classification method, which satisfies the requirements of our research [28]. Therefore, the development of new technologies such as big data, crowdsourcing, and cloud computing provides convenience for researchers to collect high-quality datasets [21,46].

As mentioned before, three metropolises, Beijing, Shanghai, and Shenzhen, were selected as study areas with the assumption that they would have huge differences in their urban fabric. Accordingly, the results in Section 3.1 indicate that both the composition and spatial configuration of LCZs had obvious differences, which is consistent with the results of previous studies. For the composition differences, compact LCZs 2 and 3 were

the dominant LCZ types for Beijing, while open LCZs 4 and 5 had the largest coverage in Shanghai. In addition, the area percentage of high-building LCZ types in Shanghai was higher than in Beijing. As a result, compared with Shanghai, Beijing was a city that had higher building density and lower building height. The possible reason was that Beijing has a long history with plenty of ancient buildings, such as "Hutong", that need to be preserved. Furthermore, as the political and cultural center, development and urban planning are easily influenced by policies. Differently from Beijing and Shanghai, Shenzhen is a quite newly emerged city, and its special and biggest feature was that it had a very high area of LCZ A. In addition, the spatial distribution of vegetation in Shenzhen is not concentrated in the outside of downtown as in Beijing and Shanghai. It is easy to find a large area of vegetation in the central part of Shenzhen, which is rare to see in the other two cities. These differences of urban spatial structure might be due to the two aspects: natural factors (such as location, topography, and climate) and social ones (e.g., history, culture, and urban planning) [47–49]. It is believed that these variations in LCZ could produce differences in the thermal environment.

4.2. Differences in the Urban Thermal Environment

Despite the Landsat 8 TIRS images being selected on clear days in summer with similar weather, the spatial and statistical characteristics of LST still had substantial differences among these three cities, which was consistent with previous studies [33,48,50]. The basic difference was that Shenzhen had the highest average LST, while Beijing had the smallest. That was because Shenzhen was located in a tropical area. Therefore, it could be inferred that the climate background determined the differences in the thermal environment. In addition, Shenzhen had the strongest SUHI intensity among the three cities. It seemed that Shenzhen had the worst thermal environment based on the SUHI intensity. However, it should be noted the SUHI intensity was merely a LST difference between certain LCZ types, which could not represent the spatial features of the thermal environment. Therefore, reclassified LST maps were made by ArcGIS based on the relationship between the mean LST and corresponding standard deviation. Five LST categories named highest, high, medium, low, and lowest were applied in this study, which represented relative LST for each city (Figure 7). The SUHI region was defined as the sum area of the highest and high zones whose LSTs were higher than the average values, while the SUCI (surface urban cooling island) was the area of the low and lowest with lower LSTs. The spatial patterns of reclassified LST are shown in Figure 7.

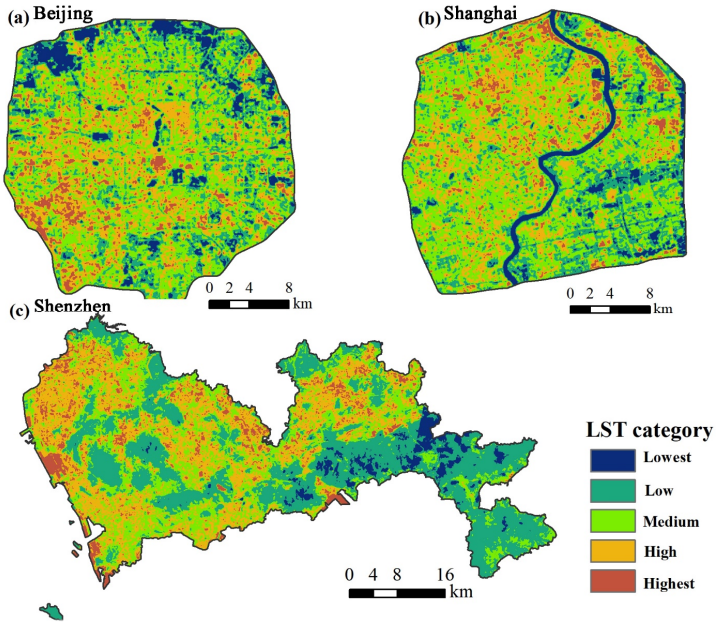


Figure 7. Spatial patterns of reclassified LST in (**a**) Beijing, (**b**) Shanghai, and (**c**) Shenzhen.

Calculating the area of SUHI and SUCI region indicated that Shenzhen still had the largest area percentage (35.72%) of SUHI and was followed by Shanghai (32.33%) and Beijing (28.01%). It was clear that the high and highest LST in Shenzhen were mainly concentrated in the compact built-up areas shown in Figures 2c and 7c, although it had a large area of vegetation. However, an interesting thing was that the area proportion of SUCI in Shenzhen was still the largest and was much higher than in Beijing and Shanghai. In other words, Shenzhen had the smallest area proportion of medium LST. Beijing and Shanghai had similar SUHI intensities and spatial patterns of the urban thermal environment in summer, which was quite different from Shenzhen, which had the strongest SUHI intensity and largest area proportion of SUHI region. These results are similar to previous studies, which further suggests that tropic cities face a higher thermal stress and risk [51,52].

4.3. Effects of LCZ on the LST

In this study, the LCZs were taken as the basic composition elements in a 1 × 1 km grid to explore their relationships with LST, which was an innovation of the research method. Compared to previous studies, similar results were also found, e.g., the LST of built-up LCZs were typically higher than land cover ones due to the physical and optical properties in both coastal and inland cities [31,53–55]. It is well known that buildings easily absorb more solar radiation, and vegetation has a cooling effect due to its shade and evapotranspiration [39,56].

However, in addition to these common conclusions, several interesting and new results were found in this study. The intensity of the relationships between LCZ and LST had obvious variations among LCZ types and the three studied cities. For the variations among LCZ types, we found the compact-built LCZs such as LCZs 2 and 3 had higher correlation coefficients than open-rise buildings, indicating they might have a stronger effect on LST, which was consistent with previous studies in which higher UHI intensity was observed in built-up LCZs in Guangzhou, China [31,53,57]. For land cover LCZ types, LCZA had the largest negative correlation coefficient with LST in Beijing and Shenzhen. For the differences in correlations among cities, it was found that the relationships were much stronger in Shenzhen than in Beijing and Shanghai. One possible reason was that the spatial characteristics of LCZs including composition components and configuration had similar features in Beijing and Shanghai but were quite different from Shenzhen.

Multi-linear regression models can compare the relative contributions of different LCZ to LST, which can help determine the dominant impact factors on LST [12,58]. For Beijing city, the results of the regression models showed that the coefficients of built-up LCZ types such LCZs 2 and 3 were larger than land cover LCZ, which indicated that the warming effect of man-made buildings (impervious surfaces) was stronger than the cooling effect produced by natural LCZs. However, things changed in Shanghai where the cooling effect of the water body was much stronger than the warming effect generated by built LCZs. In Shenzhen, the relative contribution of LCZ A to LST was much higher than other LCZ types. Therefore, it could be concluded that the urban thermal environment of Beijing was easily influenced by artificial buildings and surfaces, while the variations of LST in the coastal cities Shanghai and Shenzhen were dominated by water and dense trees, respectively. As a result, these findings might provide a scientific basis for decision-makers for urban planning from the perspective of regulating urban climate.

4.4. Limitations and Future Research

It should be noted that there are still some limitations in this study. First, as the LST changes all the time, seasonal and daily variations of LST should be explored in future studies by using multi-sources such as MODIS and unmanned aerial vehicle monitoring. Second, only three metropolises were selected as study areas. However, more cities with different LCZ characteristics should be considered to obtain more comprehensive results. Finally, traditional statistical analysis was used to explore the relationships between LCZ

and LST. With the rapid development of machine learning, some deep learning methods such as XGBoost might yield interesting results [59].

5. Conclusions

In order to compare the variations of relationships between LCZ and LST among different cities at fine spatial scales, Beijing, Shanghai, and Shenzhen were selected as the study areas. In addition, LCZ maps and Landsat 8 images were used to characterize the urban features and thermal conditions, respectively. Our results indicated the following:

(1) Both the landscape components and spatial configurations of LCZs had obvious differences in these three cities. In particular, Beijing was a denser city with more compact low-rise buildings, and Shanghai had a higher area proportion of open high-rise LCZs, with Shenzhen having a much higher vegetation coverage;
(2) For differences in the urban thermal environment, Shenzhen had the strongest SUHI intensity among the three cities and the largest area proportion of the SUHI region. However, Shenzhen still had the largest area percentage of UCI due to the high coverage of LCZ A;
(3) The LST differences among LCZ types were huge, and typically, the built-up LCZs had higher LSTs than land cover types in all these three cities, but Beijing and Shanghai had similar variations that were quite different from Shenzhen;
(4) For the effects of LCZ on LST, it was found that these three cities had their different dominant LCZs in determining the changes of LST. The LST in Beijing was more easily influenced by compact-built LCZs such as LCZs 2 and 3, while LCZ G had a much stronger influence on LST in Shanghai. LCZ A had the largest contribution to the variation of LST in Shenzhen. As a result, different characteristics of LCZ in these three cities contributed to the variations of LST, indicating that the effect of LCZ on the urban thermal environment was profound.

The findings in this study add to our understanding of the relationships between LCZ and the thermal environment, thus providing a scientific basis for urban planners and decision-makers.

Author Contributions: Conceptualization, Chaobin Yang; methodology, Riguga Su; software, Lilong Yang; validation, Lifeng Liu; formal analysis, Zhibo Xu; investigation, Riguga Su; resources, Tingwen Luo; data curation, Zhibo Xu; writing—original draft preparation, Riguga Su; writing—review & editing, Chaobin Yang; visualization, Lilong Yang and Chao Wang; supervision, Chaobin Yang; funding acquisition, Tingwen Luo. All authors have read and agreed to the published version of the manuscript.

Funding: This study was funded by the National Natural Science Foundation of China (grant number 42201123) and the China Postdoctoral Science Foundation (grant number 2022M713309). This study was also supported by the Open Fund of the Key Laboratory of Urban Land Resources Monitoring and Simulation (KF-2022-07-002), Ministry of Natural Resources, and the Opening Fund of State Key Laboratory of Green Building in Western China with Project Number: (LSKF202308).

Data Availability Statement: The data presented in this study are available on request from the corresponding author.

Conflicts of Interest: The authors declare no conflicts of interest.

References

1. Sharifi, A.; Pathak, M.; Joshi, C.; He, B.-J. A Systematic Review of the health co-benefits of urban climate change adaptation. *Sustain. Cities Soc.* **2021**, *398*, 698–708. [CrossRef]
2. Ebi, K.L.; Capon, A.; Berry, P.; Broderick, C.; de Dear, R.; Havenith, G.; Honda, Y.; Kovats, R.S.; Ma, W.; Malik, A.; et al. Hot weather and heat extremes: Health risks. *Lancet* **2021**, *398*, 698–708. [CrossRef]
3. Chen, M.; Chen, L.; Zhou, Y.; Hu, M.; Jiang, Y.; Huang, D.; Gong, Y.; Xian, Y. Rising vulnerability of compound risk inequality to ageing and extreme heatwave exposure in global cities. *Npj Urban Sustain.* **2023**, *3*, 38. [CrossRef]
4. Arnfield, A.J. Two decades of urban climate research: A review of turbulence, exchanges of energy and water, and the urban heat island. *Int. J. Climatol.* **2003**, *23*, 1–26. [CrossRef]

5. Rizvi, S.H.; Alam, K.; Iqbal, M.J. Spatio-temporal variations in urban heat island and its interaction with heat wave. *J. Atmos. Sol.-Terr. Phys.* **2019**, *185*, 50–57. [CrossRef]
6. He, B.-J.; Wang, J.; Zhu, J.; Qi, J. Beating the urban heat: Situation, background, impacts and the way forward in China. *Renew. Sustain. Energy Rev.* **2022**, *161*, 112350. [CrossRef]
7. Ellena, M.; Melis, G.; Zengarini, N.; Di Gangi, E.; Ricciardi, G.; Mercogliano, P.; Costa, G. Micro-scale UHI risk assessment on the heat-health nexus within cities by looking at socio-economic factors and built environment characteristics: The Turin case study (Italy). *Urban Clim.* **2023**, *49*, 101514. [CrossRef]
8. Levermore, G.; Parkinson, J.; Lee, K.; Laycock, P.; Lindley, S. The increasing trend of the urban heat island intensity. *Urban Clim.* **2017**, *24*, 360–368. [CrossRef]
9. Rizwan, A.M.; Dennis, L.Y.C.; Liu, C. A review on the generation, determination and mitigation of Urban Heat Island. *J. Environ. Sci.* **2008**, *20*, 120–128. [CrossRef]
10. Zhou, D.; Xiao, J.; Bonafoni, S.; Berger, C.; Deilami, K.; Zhou, Y.; Frolking, S.; Yao, R.; Qiao, Z.; Sobrino, J. Satellite Remote Sensing of Surface Urban Heat Islands: Progress, Challenges, and Perspectives. *Remote Sens.* **2018**, *11*, 48. [CrossRef]
11. Yang, C.; Kui, T.; Zhou, W.; Fan, J.; Pan, L.; Wu, W.; Liu, M. Impact of refined 2D/3D urban morphology on hourly air temperature across different spatial scales in a snow climate city. *Urban Clim.* **2023**, *47*, 101404. [CrossRef]
12. Huang, X.; Wang, Y. Investigating the effects of 3D urban morphology on the surface urban heat island effect in urban functional zones by using high-resolution remote sensing data: A case study of Wuhan, Central China. *ISPRS J. Photogramm. Remote Sens.* **2019**, *152*, 119–131. [CrossRef]
13. Peng, X.; Zhou, Y.; Fu, X.; Xu, J. Study on the spatial-temporal pattern and evolution of surface urban heat island in 180 shrinking cities in China. *Sustain. Cities Soc.* **2022**, *84*, 104018. [CrossRef]
14. Yang, C.; Yan, F.; Lei, X.; Ding, X.; Zheng, Y.; Liu, L.; Zhang, S. Investigating Seasonal Effects of Dominant Driving Factors on Urban Land Surface Temperature in a Snow-Climate City in China. *Remote Sens.* **2020**, *12*, 3006. [CrossRef]
15. Yang, Q.; Huang, X.; Tang, Q. The footprint of urban heat island effect in 302 Chinese cities: Temporal trends and associated factors. *Sci. Total Environ.* **2019**, *655*, 652–662. [CrossRef]
16. Weng, Q. Thermal infrared remote sensing for urban climate and environmental studies: Methods, applications, and trends. *ISPRS J. Photogramm. Remote Sens.* **2009**, *64*, 335–344. [CrossRef]
17. Weng, Q.; Lu, D.; Schubring, J. Estimation of land surface temperature–vegetation abundance relationship for urban heat island studies. *Remote Sens. Environ.* **2004**, *89*, 467–483. [CrossRef]
18. Roy, D.P.; Wulder, M.A.; Loveland, T.R.; Woodcock, C.E.; Allen, R.G.; Anderson, M.C.; Helder, D.; Irons, J.R.; Johnson, D.M.; Kennedy, R.; et al. Landsat-8: Science and product vision for terrestrial global change research. *Remote Sens. Environ.* **2014**, *145*, 154–172. [CrossRef]
19. Zhang, X.; Du, S.; Wang, Q. Hierarchical semantic cognition for urban functional zones with VHR satellite images and POI data. *ISPRS J. Photogramm. Remote Sens.* **2017**, *132*, 170–184. [CrossRef]
20. Mitz, E.; Kremer, P.; Larondelle, N.; Stewart, J. Structure of Urban Landscape and Surface Temperature: A Case Study in Philadelphia, PA. *Front. Environ. Sci.* **2021**, *9*, 592716. [CrossRef]
21. Cao, R.; Tu, W.; Yang, C.; Li, Q.; Liu, J.; Zhu, J.; Zhang, Q.; Li, Q.; Qiu, G. Deep learning-based remote and social sensing data fusion for urban region function recognition. *ISPRS J. Photogramm. Remote Sens.* **2020**, *163*, 82–97. [CrossRef]
22. Stewart, I.D.; Oke, T.R. Local Climate Zones for Urban Temperature Studies. *Bull. Am. Meteorol. Soc.* **2012**, *93*, 1879–1900. [CrossRef]
23. Hidalgo, J.; Dumas, G.; Masson, V.; Petit, G.; Bechtel, B.; Bocher, E.; Foley, M.; Schoetter, R.; Mills, G. Comparison between local climate zones maps derived from administrative datasets and satellite observations. *Urban Clim.* **2019**, *27*, 64–89. [CrossRef]
24. Yoo, C.; Han, D.; Im, J.; Bechtel, B. Comparison between convolutional neural networks and random forest for local climate zone classification in mega urban areas using Landsat images. *ISPRS J. Photogramm. Remote Sens.* **2019**, *157*, 155–170. [CrossRef]
25. La, Y.; Bagan, H.; Yamagata, Y. Urban land cover mapping under the Local Climate Zone scheme using Sentinel-2 and PALSAR-2 data. *Urban Clim.* **2020**, *33*, 100661. [CrossRef]
26. Huang, F.; Jiang, S.; Zhan, W.; Bechtel, B.; Liu, Z.; Demuzere, M.; Huang, Y.; Xu, Y.; Ma, L.; Xia, W.; et al. Mapping local climate zones for cities: A large review. *Remote Sens. Environ.* **2023**, *292*, 113573. [CrossRef]
27. Fonte, C.C.; Lopes, P.; See, L.; Bechtel, B. Using OpenStreetMap (OSM) to enhance the classification of local climate zones in the framework of WUDAPT. *Urban Clim.* **2019**, *28*, 100456. [CrossRef]
28. Demuzere, M.; Kittner, J.; Bechtel, B. LCZ Generator: A Web Application to Create Local Climate Zone Maps. *Front. Environ. Sci.* **2021**, *9*, 637455. [CrossRef]
29. Aslam, A.; Rana, I.A. The use of local climate zones in the urban environment: A systematic review of data sources, methods, and themes. *Urban Clim.* **2022**, *42*, 101120. [CrossRef]
30. Leconte, F.; Bouyer, J.; Claverie, R.; Pétrissans, M. Using Local Climate Zone scheme for UHI assessment: Evaluation of the method using mobile measurements. *Build. Environ.* **2015**, *83*, 39–49. [CrossRef]
31. Chen, G.; Chen, Y.; He, H.; Wang, J.; Zhao, L.; Cai, Y. Assessing the synergies between heat waves and urban heat islands of different local climate zones in Guangzhou, China. *Build. Environ.* **2023**, *240*, 110434. [CrossRef]
32. Ferreira, L.S.; Duarte, D.H.S. Exploring the relationship between urban form, land surface temperature and vegetation indices in a subtropical megacity. *Urban Clim.* **2019**, *27*, 105–123. [CrossRef]

33. Bechtel, B.; Demuzere, M.; Mills, G.; Zhan, W.; Sismanidis, P.; Small, C.; Voogt, J. SUHI analysis using Local Climate Zones—A comparison of 50 cities. *Urban Clim.* **2019**, *28*, 100451. [CrossRef]
34. Kotharkar, R.; Bagade, A. Evaluating urban heat island in the critical local climate zones of an Indian city. *Landsc. Urban Plan.* **2018**, *169*, 92–104. [CrossRef]
35. Zheng, Y.; Ren, C.; Shi, Y.; Yim, S.H.L.; Lai, D.Y.F.; Xu, Y.; Fang, C.; Li, W. Mapping the spatial distribution of nocturnal urban heat island based on Local Climate Zone framework. *Build. Environ.* **2023**, *234*, 110197. [CrossRef]
36. Ma, L.; Yang, Z.; Zhou, L.; Lu, H.; Yin, G. Local climate zones mapping using object-based image analysis and validation of its effectiveness through urban surface temperature analysis in China. *Build. Environ.* **2021**, *206*, 108348. [CrossRef]
37. Yuan, B.; Zhou, L.; Hu, F.; Zhang, Q. Diurnal dynamics of heat exposure in Xi'an: A perspective from local climate zone. *Build. Environ.* **2022**, *222*, 109400. [CrossRef]
38. Nasehi, S.; Yavari, A.; Salehi, E.; Emmanuel, R. Role of local climate zone and space syntax on land surface temperature (case study: Tehran). *Urban Clim.* **2022**, *45*, 101245. [CrossRef]
39. Zhang, J.; Li, Z.; Wei, Y.; Hu, D. The impact of the building morphology on microclimate and thermal comfort-a case study in Beijing. *Build. Environ.* **2022**, *223*, 109469. [CrossRef]
40. Jiang, L.; Liu, S.; Liu, C.; Feng, Y. How do urban spatial patterns influence the river cooling effect? A case study of the Huangpu Riverfront in Shanghai, China. *Sustain. Cities Soc.* **2021**, *69*, 102835. [CrossRef]
41. Alexander, C. Normalised difference spectral indices and urban land cover as indicators of land surface temperature (LST). *Int. J. Appl. Earth Obs. Geoinf.* **2020**, *86*, 102013. [CrossRef]
42. Sobrino, J.A.; Jiménez-Muñoz, J.C.; Paolini, L. Land surface temperature retrieval from LANDSAT TM 5. *Remote Sens. Environ.* **2004**, *90*, 434–440. [CrossRef]
43. USGS. *Landsat 8 Hand Book*; U.S. Geological Survey: Reston, VA, USA, 2016.
44. Yang, C.; Yan, F.; Zhang, S. Comparison of land surface and air temperatures for quantifying summer and winter urban heat island in a snow climate city. *J. Environ. Manag.* **2020**, *265*, 110563. [CrossRef] [PubMed]
45. Sheng, L.; Tang, X.; You, H.; Gu, Q.; Hu, H. Comparison of the urban heat island intensity quantified by using air temperature and Landsat land surface temperature in Hangzhou, China. *Ecol. Indic.* **2017**, *72*, 738–746. [CrossRef]
46. Zhou, Y.; Zhang, G.; Jiang, L.; Chen, X.; Xie, T.; Wei, Y.; Xu, L.; Pan, Z.; An, P.; Lun, F. Mapping local climate zones and their associated heat risk issues in Beijing: Based on open data. *Sustain. Cities Soc.* **2021**, *74*, 103174. [CrossRef]
47. Yang, J.; Xin, J.; Zhang, Y.; Xiao, X.; Xia, J. Contributions of sea-land breeze and local climate zones to daytime and nighttime heat island intensity. *Npj Urban Sustain.* **2022**, *2*, 12. [CrossRef]
48. Unal Cilek, M.; Cilek, A. Analyses of land surface temperature (LST) variability among local climate zones (LCZs) comparing Landsat-8 and ENVI-met model data. *Sustain. Cities Soc.* **2021**, *69*, 102877. [CrossRef]
49. Li, Y.; Sun, Y.; Li, J.; Gao, C. Socioeconomic drivers of urban heat island effect: Empirical evidence from major Chinese cities. *Sustain. Cities Soc.* **2020**, *63*, 102425. [CrossRef]
50. Wang, R.; Voogt, J.; Ren, C.; Ng, E. Spatial-temporal variations of surface urban heat island: An application of local climate zone into large Chinese cities. *Build. Environ.* **2022**, *222*, 109378. [CrossRef]
51. Yi, T.; Wang, H.; Liu, C.; Li, X.; Wu, J. Thermal comfort differences between urban villages and formal settlements in Chinese developing cities: A case study in Shenzhen. *Sci. Total Environ.* **2022**, *853*, 158283. [CrossRef]
52. Zou, Z.; Yan, C.; Yu, L.; Jiang, X.; Ding, J.; Qin, L.; Wang, B.; Qiu, G. Impacts of land use/land cover types on interactions between urban heat island effects and heat waves. *Build. Environ.* **2021**, *204*, 108138. [CrossRef]
53. Ma, L.; Huang, G.; Johnson, B.A.; Chen, Z.; Li, M.; Yan, Z.; Zhan, W.; Lu, H.; He, W.; Lian, D. Investigating urban heat-related health risks based on local climate zones: A case study of Changzhou in China. *Sustain. Cities Soc.* **2023**, *91*, 104402. [CrossRef]
54. Du, P.; Chen, J.; Bai, X.; Han, W. Understanding the seasonal variations of land surface temperature in Nanjing urban area based on local climate zone. *Urban Clim.* **2020**, *33*, 100657. [CrossRef]
55. Ren, J.; Yang, J.; Zhang, Y.; Xiao, X.; Xia, J.C.; Li, X.; Wang, S. Exploring thermal comfort of urban buildings based on local climate zones. *J. Clean. Prod.* **2022**, *340*, 130744. [CrossRef]
56. Pamukcu-Albers, P.; Ugolini, F.; La Rosa, D.; Grădinaru, S.R.; Azevedo, J.C.; Wu, J. Building green infrastructure to enhance urban resilience to climate change and pandemics. *Landsc. Ecol.* **2021**, *36*, 665–673. [CrossRef]
57. Chen, G.; Chen, Y.; Tan, X.; Zhao, L.; Cai, Y.; Li, L. Assessing the urban heat island effect of different local climate zones in Guangzhou, China. *Build. Environ.* **2023**, *244*, 110770. [CrossRef]
58. Yang, C.; Zhu, W.; Sun, J.; Xu, X.; Wang, R.; Lu, Y.; Zhang, S.; Zhou, W. Assessing the effects of 2D/3D urban morphology on the 3D urban thermal environment by using multi-source remote sensing data and UAV measurements: A case study of the snow-climate city of Changchun, China. *J. Clean. Prod.* **2021**, *321*, 128956. [CrossRef]
59. Yu, S.; Chen, Z.; Yu, B.; Wang, L.; Wu, B.; Wu, J.; Zhao, F. Exploring the relationship between 2D/3D landscape pattern and land surface temperature based on explainable eXtreme Gradient Boosting tree: A case study of Shanghai, China. *Sci. Total Environ.* **2020**, *725*, 138229. [CrossRef]

Disclaimer/Publisher's Note: The statements, opinions and data contained in all publications are solely those of the individual author(s) and contributor(s) and not of MDPI and/or the editor(s). MDPI and/or the editor(s) disclaim responsibility for any injury to people or property resulting from any ideas, methods, instructions or products referred to in the content.